Engineering Structures 226 (2021) 111340

Contents lists available at ScienceDirect

Engineering Structures

journal homepage: www.elsevier.com/locate/engstruct

Shear capacity prediction of stiffened steel plate shear walls (SSPSW) with openings using response surface method

Maryam Bypour [a], Mahdi Kioumarsi [b,*], Mohammad Yekrangnia [c]

[a] Faculty of Civil Engineering, Semnan University, Semnan, Iran
[b] Department of Civil Engineering and Energy Technology, OsloMet – Oslo Metropolitan University, Oslo, Norway
[c] Department of Civil Engineering, Shahid Rajaee Teacher Training University, Tehran, Iran

ARTICLE INFO

Keywords:
Stiffened steel plate shear wall (SSPSW)
Finite element (FE)
Response surface method (RSM)
Opening
Stiffener

ABSTRACT

In this study, nonlinear finite element (NLFE) analysis is conducted to determine the maximum shear capacity (V_{max}) of stiffened steel plate shear walls (SSPSW) with rectangular openings. Results of a wide range of parametric study are presented using developed response surface method (RSM), which quantified the effect of prominent input variables on the predicted shear capacity of SSPSW. The studied parameters, which evaluated by different aspect ratios of the infill plate (L/h), are thickness of the infill plate (t), yield stress of the steel used in the infill plate (F_y), and the ratio of opening area to the total area of the infill plate (A_o/A_p). RSM is utilized to propose equations to predict the maximum shear capacity of SSPSW with different rectangular opening ratios, which can assist in optimum designing of SSPSW. Results show that, RSM is an accurate method to predict the shear capacity of specimens. Furthermore, by having characteristics of the specimens, the optimum size of openings and thickness of the infill plate can be calculated to achieve the target V_{max}. Evaluating the results also indicated that shear capacity has linear relationship with variations of the steel infill plate thickness. Besides, by increasing in the thickness and aspect ratio of the infill plate, V_{max} is strongly influenced by opening ratio.

1. Introduction

In the last four decades, steel plate shear walls (SPSWs) have been used as one of the lateral load resisting systems in high seismic areas [1]. Desirable performance of SPSW in increasing the load-carrying capacity, stiffness, ductility and energy dissipation capacity of structures has led to widespread use of this system [2–6]. SPSW transfers lateral seismic loads to boundary frame through tension field action of infill plate. In unstiffened thin SPSW, buckling capacity is low, and after the buckling of web plate on one diagonal, a tension field develops along the opposite diagonal. Using stiffened SPSW (SSPSW) is developed to ensure that the infill plate attains full plastic strength before out-of-plane buckling [7].

In some cases, due to constructional problems such as welding, it is essential to use thicker infill plates. Doing so can result in an increase in the activated forces from the infill plate applied to the boundary frame, which requires increasing the size of the boundary frame members. To avoid this, the capacity of the infill plate should be controlled [1]. The possible damaging effects of the infill plate to the boundary frame have been investigated in several studies in the form of using low yield point (LYP) [8], light-gauge and cold-rolled steel for infill plate [9]. In addition, introduction of the regular layout of circular perforations is used as an effective way to control the capacity of the infill plate [1].

So far, the available proposed equations for SPSW with openings are utilizable for SPSW with circular openings. For instance, the equation presented in AISC 341-10 [1], is applicable for SPSW with regular layout of circular perforations. Given the fact that there are numerous SPSW with rectangular opening, it is necessary to propose equations for rectangular openings. With regards to the geometry and size of the openings, the thickness and material of the infill plate are variable; it is essential to investigate other methods for estimating the response characteristics of SPSW. In this study several numerical models are analyzed by applying nonlinear finite element (NLFE) method. The parameters under study are thickness (t), yield strength (F_y), and ratio of the opening area to the total area of the steel infill plate (A_o/A_p). Moreover, response surface method (RSM) is utilized to propose equations to predict the maximum shear capacity (V_{max}) of SSPSW with rectangular openings.

2. Background

Many experimental and numerical studies have been carried out to

* Corresponding author.
E-mail addresses: mbypour@alum.semnan.ac.ir (M. Bypour), mahdik@oslomet.no (M. Kioumarsi), yekrangnia@sru.ac.ir (M. Yekrangnia).

https://doi.org/10.1016/j.engstruct.2020.111340
Received 16 March 2020; Received in revised form 1 August 2020; Accepted 14 September 2020
Available online 10 October 2020

investigate the effects of opening on the behavior of SPSW, which result in proposing formulas to predict the shear capacity [10–16]. Roberts and Sabouri-Ghomi [10] conducted experimental investigation on unstiffened SPSW with a circular perforation on the center of steel panel (see Fig. 1(a)). They proposed formula to predict the strength and stiffness of circular perforated SPSW by introduction of reduction factors as Eq. (1).

$$\frac{V_{yp\ perf}}{V_{yp}} = \frac{K_{perf}}{K_{panel}} = \left[1 - \frac{D}{h}\right] \tag{1}$$

where $\frac{V_{yp\ perf}}{V_{yp}}$ and $\frac{K_{perf}}{K_{panel}}$ are the ratios of strength and stiffness of perforated panel to corresponding solid panel, respectively; D and h are the diameter of opening and the height of panel, respectively. Vian and Bruneau [11] upgraded the equations suggested by Roberts and Sabouri-Ghomi [10] for estimating the stiffness reduction factor of SPSW with multiple circular perforations (see Fig. 1(b)) according to Eq. (2).

$$\frac{K_{perf}}{K_{panel}} = \frac{1 - \frac{\pi}{4}\left[\frac{D}{S_{diag}}\right]}{1 - \frac{\pi}{4}\left[\frac{D}{S_{diag}}\right]\left[1 - \frac{N_r D \sin\alpha}{H_C}\right]} \tag{2}$$

where D is the diameter of the perforations; S_{diag} is the shortest center-to-center distance between the perforations; H_C is clear column height between flanges of the beams; N_r is the number of horizontal rows of perforations; and α (in degrees) is the vertical angle of the shortest center-to-center lines in the opening array.

According to the AISC 341-10 [1], the stiffness of SPSW with regular layout of circular perforations, can be calculated by Eq. (2). It should be noted that, in the AISC 341-10 [1] $\frac{t_{eff}}{t_w}$ is used instead of $\frac{K_{perf}}{K_{panel}}$ in Eq. (2).

Bhowmick et al. [12], by conducting an analytical study, based on strip model, proposed an equation to predict the shear strength of unstiffened SPSW with multiple circular openings. NLFE models with eight different types of perforation patterns were performed to investigate the accuracy of the proposed equation. The results of the proposed equation and the NLFE analysis exhibited excellent agreement. Meghdadian et al. [13] carried out a numerical study on the composite steel plate shear walls (CSPSWs) with opening. Combining their results with Multi-Expression Programming (MEP) led to an empirical equation to determine equivalent reduced thickness as a substitute of direct modeling of the opening. A parametric FE analysis on several unstiffened SPSW with opening has been performed by Formisano et al. [14]. The studied parameters were the number and diameter of the openings, the plate thickness and the material properties. An analytical tool was developed for estimation the strength and stiffness of such SPSW. Meghdadian and Ghalehnovi [15,16] conducted experimental and numerical studies to investigate the behavior of solid and perforated CSPSW. Based on the results, a relation was proposed to determine lateral displacements and ultimate strength of the perforated CSPSW, which can be used to determine displacement of the perforated CSPSW from that in the corresponding solid CSPSW.

Many researches were carried out to investigate the effect of various parameters on the behavior of different types of SPSW with openings [17–23]. Alavi and Nateghi [18] experimentally studied the seismic performance of diagonally stiffened SPSW with single-central circular opening. The results demonstrated that ductility ratio (μ) of the perforated specimen is about 14% larger than that of the unstiffened solid panel. Therefore, the diagonal stiffening is an appropriate strengthening method for the SPSW with a central opening. Formisano et al. [19] carried out a study on the application of SPSW with openings on seismic protection of existing reinforced concrete (RC) buildings. Different materials of low yield steel, aluminum and innovative perforated steel plates were utilized in this study. An analytical and experimental study has been performed by Nassernia and Showkati [20] to evaluate the effects of a circular opening on the behavior of specific types of tensile-braced mid-span SPSW. The results showed that, locating a single opening on the center of infill plate leads to a decrease in the strength and stiffness of the system, where this reduction has a direct correlation with the diameter of the opening. It is also shown that the shear strength of SPSW is not significantly affected by the location of openings [21–23].

3. Numerical simulation

3.1. Calibration

In this study, the experimental investigation carried out by Sabouri-Ghomi and Mamazizi [21] is used for verification of NLFE model with ABAQUS. The tested specimen was one-third scale specimen of one-story SSPSW with two rectangular openings, see Fig. 2a. The details of the selected experimental specimen, called as SSW2O2, are illustrated in Fig. 2. In this experimental test, a box frame of 60 × 30 × 2 mm was placed around the openings to prevent large deformation and to provide required stiffness and resistance against the tension field action of SPSW.

As shown in Fig. 2(b), the infill plate is divided by the stiffeners to several sub-panels. It should be noted that the moment of inertia of stiffeners and the dimensions of the sub-panels have been designed in a way that the local buckling of the sub-panels occurs earlier than the global buckling of the infill plate, and the infill plate yields before elastic buckling [21].

The material properties in different parts of the benchmark experimental specimen are presented in Table 1. The steel used for the infill plate has low yield strength and the steels of the top beam and columns have high yield strength. The other parts of the specimen are made of the ASTMA36 steel.

In the FE modeling of the specimen, quadrilateral first-order reduced integration shell elements with the size of 40 mm (S4R) was used. The

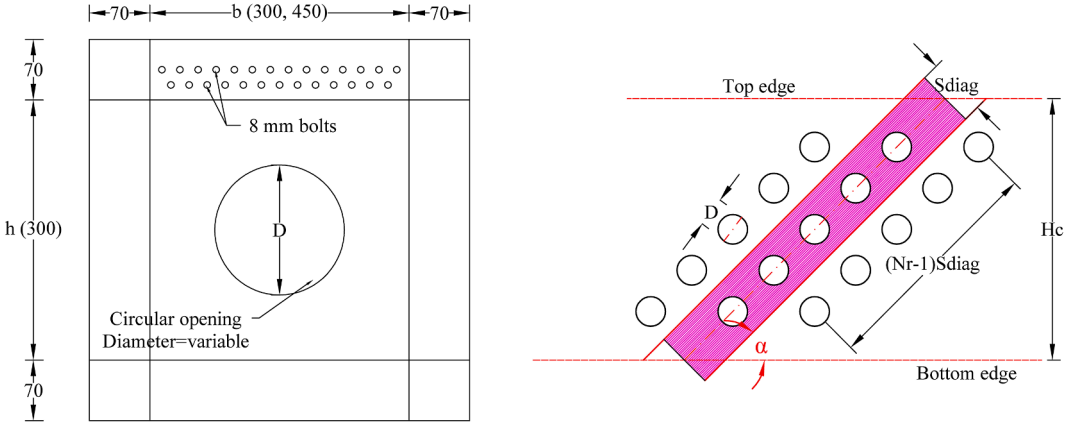

Fig. 1. The details of studied SPSW with circular opening by (a) Roberts and Sabouri-Ghomi [10], (b) Vian and Bruneau [11].

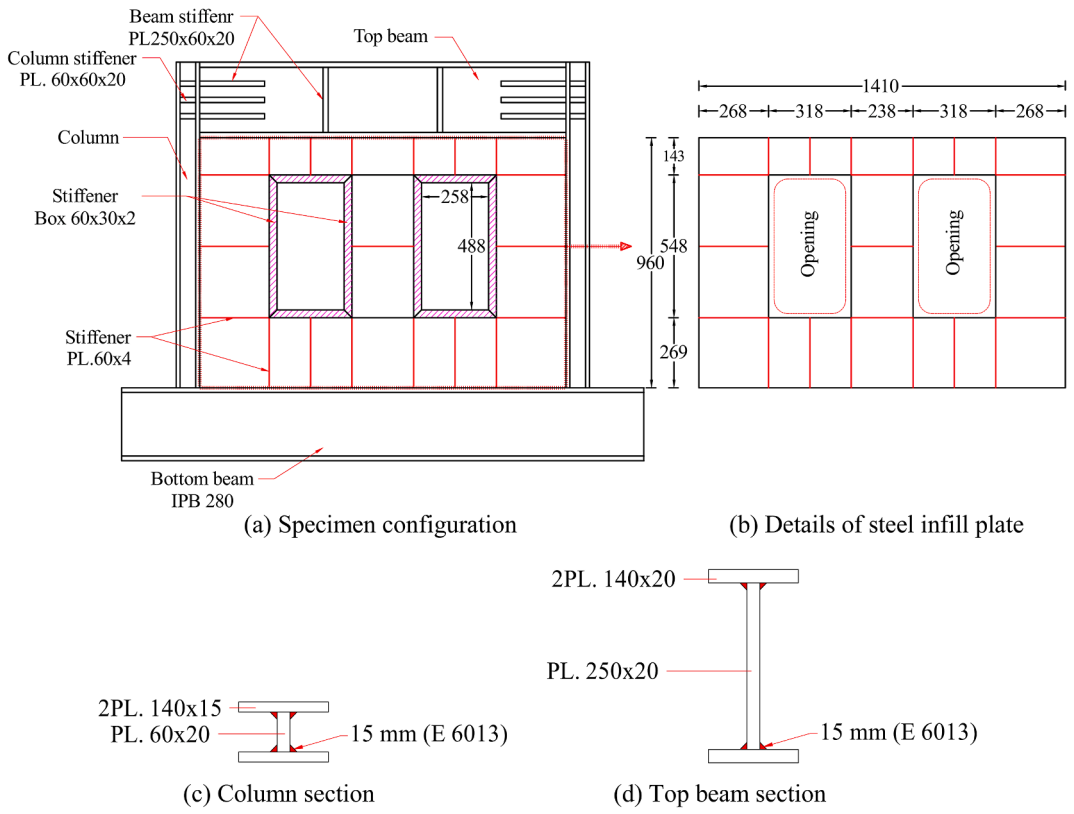

Fig. 2. Details of the experimental specimen, SSW2O2, (mm), after [21].

Table 1
Material properties of used steel in the experimental specimen, SSW2O2 and numerical simulation [21].

Members	Plate thickness (*mm*)	Yielding stress (*MPa*)	Ultimate stress (*MPa*)	Elongation (%)	Modulus of elasticity (*MPa*)
Infill plate	2	189.5	299.9	46.2	206000
Column	15	348.2	521.4	26.9	208000
Top beam	20	415.7	557.2	25.2	209000
Stiffeners	–	245.2	384.7	31.2	208000

size of the mesh, after performing mesh sensitivity analysis was determined as 40 mm. Fig. 3 illustrates the meshed FE model. In the experimental specimen, in accordance with the ATC-24 protocol [24], the cyclic quasi-static loading has been horizontally applied to the center of the top beam. Nonlinear isotropic/kinematic hardening model with ductile material damage [25] was considered for the steel.

It is noted that, since the defined material characteristics include ductile damage and significant material nonlinearity, the traditional static analysis, which includes implicit formulation e.g. Newton-Raphson, could not be utilized. Consequently, the analyses are performed using dynamic explicit method. The static nature of the applied load was ensured by considering low-rate loading and monitoring the ratio of kinetic energy to internal energy in the models at each increment. Furthermore, the difference between external work and the internal energy in the model, and at each time increment, was monitored, to maintain the numerical stability during the analyzing process. In the utilized central difference method, the numerical stability is provided when:

$$\Delta t < \frac{2}{\omega_{max-num}} \tag{3}$$

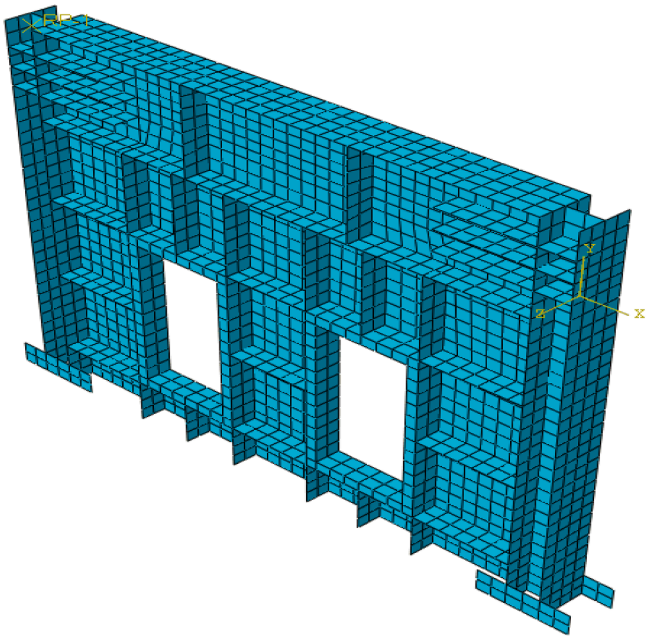

Fig. 3. The meshing size of FE model.

where Δt is the time increment and $\omega_{max-num}$ is the maximum numerical frequency of the model.

In Fig. 4, the ultimate deformation of the experimental specimen is compared with that in the FE model. As shown in this Figure, the yielding has been occurred in all sub-panels. Consequently, the rupturing of the infill plate in the FE model has good agreement with the experimental specimen. In Fig. 5, the comparison of load-displacement

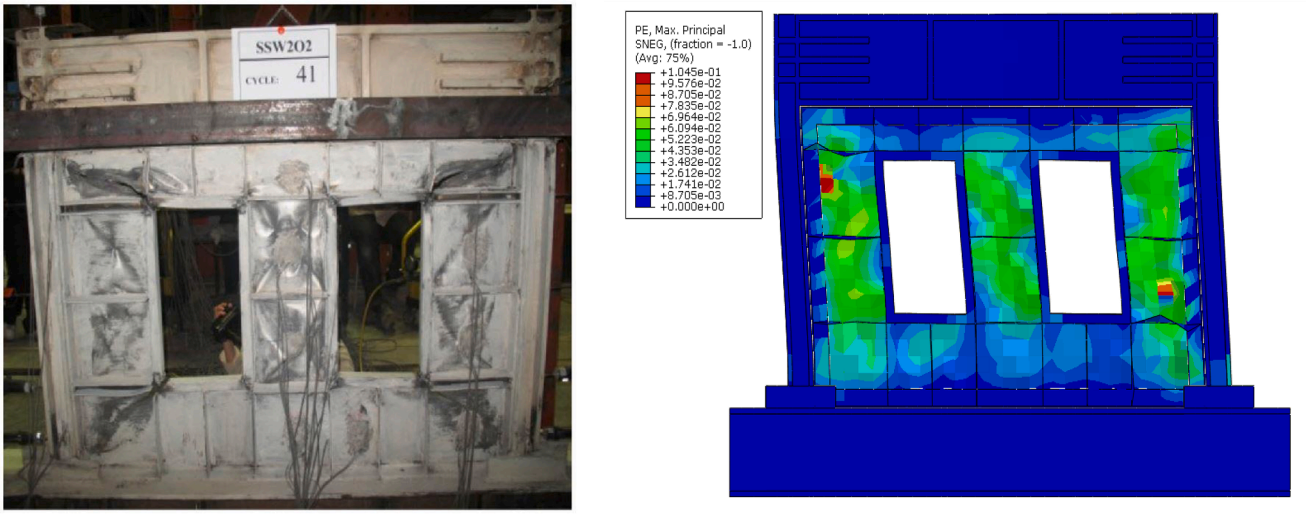

Fig. 4. Comparing of the FE analysis results with the experimental test of SSW2O2 at the ultimate displacement: (a) deformation of experimental specimen [21], and (b) maximum principal plastic strain of FE model.

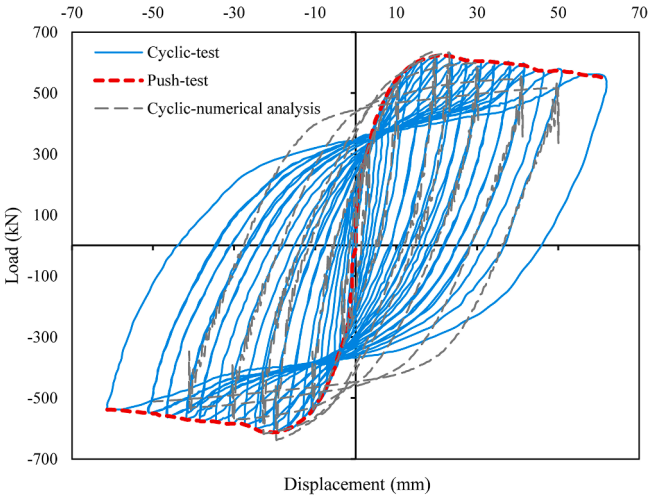

Fig. 5. Comparison of load-displacement curves of the FE analysis and the experimental test.

curves of the FE model and the experimental specimen is shown. As it can be seen in this Figure, the results of the FE model with cyclic loading have accurate conformity with the experimental specimen.

4. Response surface method (RSM)

NLFE method, used in the previous section, is an accurate tool for predicting the capacity of SPSW. However, time-consuming computational process of FE analysis is a hinder to identify interactions among the main influencing parameters in the capacity of SPSW. The use of response surface method (RSM), which is a statistical-mathematical technique for developing and optimizing processes [26], can eliminate this limitation. RSM has prominent applications in the design [27], development of new formulations and improvement of existing product designs. Recently, this method is used in civil engineering field for reliability and structural analysis [26,28–30].

In this paper, RSM is implemented to approximate and interpret the relationship between the maximum capacity of the SPSW, termed as "response" and the opening sizes, infill plate thickness, and yield strength of infill plate, termed as "variables". The approximation of this relationship or performance function is termed "response surface".

4.1. Design of response surface

In this study, the predicted response is approximated with a second-order polynomial function including the two-factor interactions between the parameters, which for k variables is expressed as Eq. (4):

$$Y = \beta_0 + \sum_{i=1}^{k} \beta_i X_i + \sum_{i=1}^{k} \beta_{ii} X_i^2 + \sum \sum_{i<1}^{k} \beta_{ij} X_i X_j \quad (4)$$

where Y is the predicted response which is the maximum shear capacity, X_i is the coded level of a design variable i, k is the total number of variables, coefficient β_0 is a constant of equation and β_i, β_{ii} and β_{ij} are the regression coefficients for the linear, quadratic and interaction effects, respectively.

The most common design method for fitting a second-order model is the central composite design (CCD). In this study, CCD method is used to fit the Eq. (4) with the obtained response data (maximum shear capacity). The total number of design points in CCD for k variables is 2^k factorial points, $2k$ axial points plus one center point. This is illustrated in Fig. 6 for three variables. In the half fractional factorial points, the number of fractional points is reduced to 2^{k-1}.

The codded distance of the axial points from the center point can obtain using the Eq. (5) [30]:

$$\alpha = \sqrt[4]{2^k} \quad (5)$$

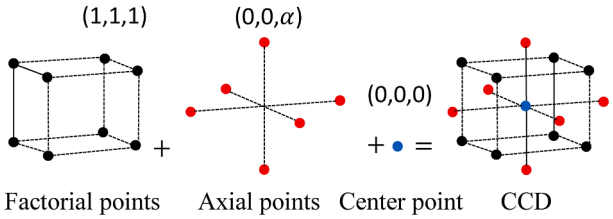

Fig. 6. Experimental design for the fitting of a second-order model when the number of variables is 3 (k = 3), using central composite design (CCD); after [30].

4.2. Variables and levels

The main purpose of using RSM is to predict the maximum shear capacity (V_{max}) of SSPSW including rectangular openings by considering the interaction effects of the influencing parameters on the capacity of SSPSW. The effect of three parameters was investigated using RSM and NLFE analysis. The studied parameters are thickness of the infill plate (t), yield stress of the steel used in the infill plate (F_y), and the ratio of opening area to the total area of the infill plate (A_o/A_p). To study the combined effects of these variables, FE analyses are implemented with various combinations of variables. Five levels for each variable must be considered in CCD: the factorial zero level ($X_i = 0$), the one level ($X_i = \pm 1$) and the axial points ($X_i = \pm\alpha$), where α equals 2 for all variables. The studied variables and their considered levels are listed in Table 2.

The minimum thickness of 1.5 mm, which is considered for the infill plate, is based on the maximum allowable slenderness ratio suggested by FEMA 450 [31] (Eq. (6)) for controlling the slenderness of the steel infill plate, in which t_w and E are thickness and modulus of elasticity of the infill plate, respectively.

$$\frac{\min(L,h)}{t_w} \le 25\sqrt{\frac{E}{F_y}} \tag{6}$$

According to the AISC-341-05 [32], the aspect ratios of infill plate (L/h), where L and h are the length and height of the infill plate, respectively, plays a prominent role in performance of SPSW. In order to consider the effect of these parameters, RSM was repeated for four different L/h ratios. AISC-341-05 [32] for the design of SPSW, suggested to limit the aspect ratio of the infill plate between 0.8 and 2.5. In this study, and in all the specimens, the height of openings was considered constant and the width of the infill plates and openings were set as variables, see Fig. 7.

4.3. Overview of the central composite design

According to central composite design, RSM with three variables requires 15 numerical experiments. Table 3 demonstrates the 15 numerical analyses, which must be performed according to CCD with three variables i.e. A_o/A_p, F_y and t. Considering the four ratios of L/h, in total, 60 specimens have been modeled and analyzed.

5. RSM results and discussions

5.1. RSM results

In this section, the predicted second-order response functions (V_{max}) from RSM regression model using coded variables with L/h of 1.47, 1.6, 2, and 2.4 are presented in Eqs. (7)–(10). As previously mentioned, the variable parameters are the thickness of the infill plate (t) in *mm*, the yield stress of steel used in the infill plate (F_y) in *MPa*, and the ratio of opening area to the total area of the infill plate (A_o/A_p) in percent (%). Consequently, the V_{max} is obtained in *kN*.

Regression model using coded variables with L/h of 1.47:

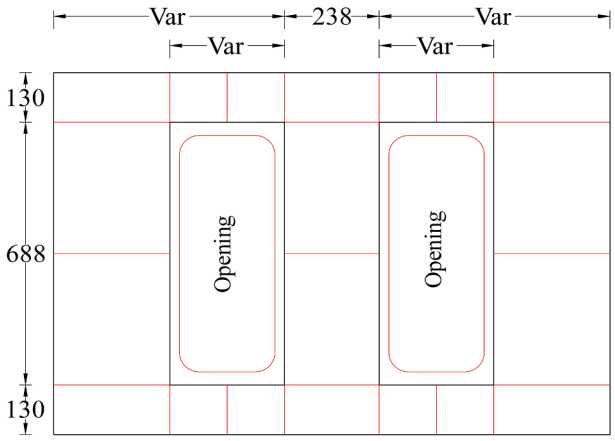

Fig. 7. Geometry of the SPSW with opening and the infill plate used in RSM (mm).

Table 3
Characteristics of models in numerical analyses, which is repeated for L/h = 1.47, 1.6, 2, and 2.4.

Run order	F_y(MPa)	t (mm)	A_o/A_p (%)
1	100	2.5	30
2	250	3	35
3	250	3	25
4	200	1.5	30
5	250	2	25
6	150	2	35
7	150	3	25
8	200	3.5	30
9	200	2.5	20
10	300	2.5	30
11	250	2	35
12	200	2.5	40
13	150	3	35
14	150	2	25
15	200	2.5	30

$$V_{max} = 66.7 + 1.690F_y + 151.2t + 4.39A_o/A_p - 0.001476F_y^2 - 8.40t^2 + 0.0052(A_o/A_p)^2 + 0.2196F_y \times t - 0.01959F_y \times A_o/A_p - 1.788t \times A_o/A_p \tag{7}$$

Regression model using coded variables with L/h of 1.6:

$$V_{max} = 62.8 + 1.556F_y + 146.9t + 6A_o/A_p - 0.001332F_y^2 - 9.38t^2 + 0.0215(A_o/A_p)^2 + 0.3071F_y \times t - 0.02096F_y \times A_o/A_p - 1.776t \times A_o/A_p \tag{8}$$

Regression model using coded variables with L/h of 2:

Table 2
Variables and their considered levels.

No.	Variables	Unit	Notation	Levels				
				Axial	Factorial			Axial
				(−2)	Low (−1)	Center (0)	High (1)	(+2)
1	Thickness	*mm*	t	1.5	2	2.5	3	3.5
2	Yielding stress	*MPa*	F_y	100	150	200	250	300
3	$A_{opening}/A_{panel}$	%	A_o/A_p	20	25	30	35	40

Table 4
Comparison of the V_{max} obtained from FE analyses and RSM.

Run order	$V_{max}(kN)$											
	$L/h = 1.47$			$L/h = 1.6$			$L/h = 2$			$L/h = 2.4$		
	FEM	RSM	Ratio*	FEM	RSM	Ratio	FEM	RSM	Ratio	FEM	RSM	Ratio
1	544.75	544.85	1.000	554.63	555.05	0.999	582.29	583.63	0.998	600.72	604.55	0.994
2	737.89	740.52	0.996	769.06	768.94	1.000	832.20	831.40	1.001	892.78	888.43	1.005
3	795.99	796.11	1.000	830.91	827.52	1.004	918.01	915.72	1.002	1006.04	996.63	1.009
4	556.50	557.82	0.998	565.82	567.07	0.998	599.90	601.98	0.997	619.10	624.50	0.991
5	675.13	676.71	0.998	696.74	695.14	1.002	759.73	758.52	1.002	815.13	809.73	1.007
6	553.04	553.68	0.999	562.76	563.94	0.998	590.84	590.16	1.001	617.30	615.63	1.003
7	666.56	669.25	0.996	686.21	685.47	1.001	746.09	745.58	1.001	797.71	794.13	1.005
8	758.60	756.78	1.002	781.53	783.35	0.998	856.25	857.76	0.998	910.89	917.90	0.992
9	703.84	703.08	1.001	718.54	721.66	0.996	794.84	796.69	0.998	860.66	867.95	0.992
10	757.62	757.03	1.001	784.85	787.48	0.997	857.94	860.19	0.997	913.62	922.05	0.991
11	640.93	639.00	1.003	655.80	654.32	1.002	699.03	696.58	1.004	738.13	730.63	1.010
12	629.09	629.36	1.000	643.26	643.22	1.000	676.17	677.91	0.997	711.74	716.85	0.993
13	634.06	633.24	1.001	648.46	647.85	1.001	690.49	688.74	1.003	727.87	722.13	1.008
14	573.68	571.81	1.003	585.89	583.80	1.004	626.78	624.62	1.003	665.26	658.53	1.010
15	666.26	665.70	1.001	681.73	684.59	0.996	733.15	736.58	0.995	768.98	781.00	0.985

* Ratio = FEM/RSM.

$$V_{max} = 72.8 + 1.888F_y + 156.1t + 4.72A_o/A_p - 0.001476F_y^2 - 6.71t^2 + 0.0072(A_o/A_p)^2 + 0.3624F_y \times t - 0.02748F_y \times A_o/A_p - 2.238t \times A_o/A_p \quad (9)$$

Regression model using coded variables with L/h of 2.4:

$$V_{max} = 115 + 2.099F_y + 180.4t + 0.12A_o/A_p - 0.00177F_y^2 - 9.8t^2 + 0.114(A_o/A_p)^2 + 0.513F_y \times t - 0.0362F_y \times A_o/A_p - 2.91t \times A_o/A_p \quad (10)$$

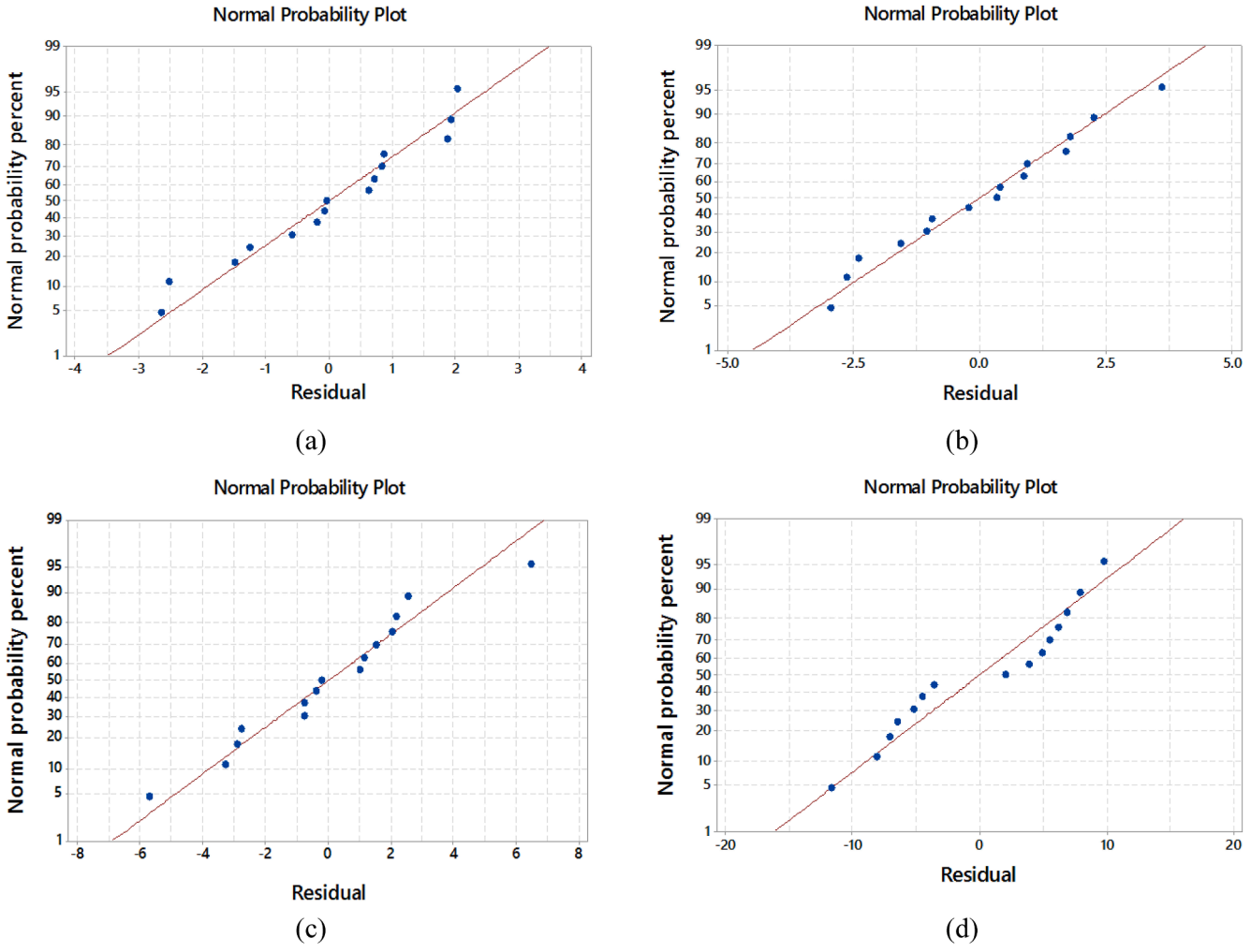

Fig. 8. Normal probability plot of residuals for V_{max}: (a) $L/h = 1.47$, (b) $L/h = 1.6$, (c) $L/h = 2$, and (d) $L/h = 2.4$.

Table 5
Characteristics of the selected random specimens to investigate the validation of RSM results (for $L/h = 1.47$, 1.6, 2, and 2.4).

Specimens	F_y(MPa)	t(mm)	A_o/A_p(%)
R1	100	2	25
R2	150	2	30
R3	200	3	35
R4	250	3	40
R5	300	4	20

Table 4 exhibits the FE analyses results and the predicted results based on Eqs. (7)–(10). As it can be seen, the results of regression models are in good match with those of the FE models within the defined levels of the variables.

Fig. 8 indicates the normal probability distribution diagram of the residuals; the difference between the obtained V_{max} by FE analyses and the predicted V_{max} by Eqs. (7)–(10). As shown in the plots, for the predicted models, the residuals are normally distributed on both sides of 0.0.

5.2. Validation of RSM results

To verify the validity of the equations obtained by RSM, a set of FE analyses was performed with random values of parameters in the defined ranges of variables. Then, the obtained FE analyses results were compared with the results obtained from the RSM (Eqs. (7)–(10)). In total, five sets of random parameters were selected for the validation, which are illustrated in Table 5. Table 6 presents comparison of the obtained results of V_{max} from FE analyses and RSM equations. Results demonstrate that, RSM can predict the V_{max} of the specimens, accurately.

5.3. Effect of parameters on V_{max}

In this section, Eqs. (7)–(10) are interpreted in terms of uncoded variables. Fig. 9 illustrates the effects of each parameter on V_{max}. The middle values for the parameters, i.e. $t = 2.5$ mm, $(A_o/A_p) = 30\%$, and $F_y = 200$ MPa, have been selected as a constant values. For comparability of the results, the graphs are presented with L/h of 1.47, 1.6, 2, and 2.4. As it can be seen in these Figures, in each L/h, the slops of all graphs approximately are the same. Also, variations of the V_{max} have linear relations with variations of the investigated parameters. Moreover, this Figure shows that, the slope of variation of the $V_{max}\left(i.e.(V_{max(L/h=2.4)} - V_{min(L/h=1.47)})/(V_{min(L/h=1.47)})\right)$ versus variations of the A_o/A_p, F_y and t are 37.90%, 69.23% and 64.55%, respectively. This indicates variations of the V_{max} is moderately more sensitive to F_y than A_o/A_p.

5.4. Optimum design

Fig. 10 illustrates the relation between $V_{\max(20\%<A_o/A_p<40\%)}$—the maximum shear capacity when the opening ratios are varied between 20 and 40%— and the steel infill plate thickness for different L/h and F_y. The results indicate that in the all considered aspect ratios, variations of the $V_{\max(20\%<A_o/A_p<40\%)}$ have linear relationship with variations of the steel infill plate thickness. In addition, with increasing the infill plate thickness, effect of variations of A_o/A_p on variations of V_{max} is more noticeable. Fig. 10 can also be used as a criterion to estimate V_{max} of a new designed specimen. Therefore, by having characteristics of specimens such as the aspect ratio of L/h and F_y, the optimum size of openings and thickness of the infill plate can be determined in order to achieve the desired V_{max}. For example, for a specimen with $L/h = 2.4$ and $F_y = 200$ MPa (see Fig. 10(f)), to reach $V_{max} = 900$ MPa, only the infill plate with $t > 2.5$ mm and $A_o/A_p < 30\%$ can be utilized. In another example, when A_o/A_p is taken as 40%, only the infill plate with $F_y = 300$ MPa (see Fig. 10(i)) is suitable and the infill plate with $F_y = 200$ MPa is not able to access the demanded V_{max}.

The incremental relative changes of the V_{max}, for each infill thickness, when the opening ratio is increased from 20% to 40% $\left(\Delta V_{max(20\%<A_o/A_p<40\%)}\right)$ for $F_y = 100$, 200 and 300 MPa and for $L/h =$

Table 6
Comparison of the results of FEM and RSM to verify the validity of the equations obtained by RSM.

Specimen	V_{max}(kN)											
	$L/h = 1.47$			$L/h = 1.6$			$L/h = 2$			$L/h = 2.4$		
	FEM	RSM	Ratio	FEM	RSM	Ratio	FEM	RSM	Ratio	FEM	RSM	Ratio
R1	517.06	508.29	**1.017**	525.87	518.14	**1.015**	553.71	546.67	**1.013**	581.56	569.65	**1.021**
R2	517.28	512.07	**1.010**	524.60	520.98	**1.007**	550.98	547.30	**1.007**	567.80	566.35	**1.003**
R3	688.64	690.57	**0.997**	712.65	711.72	**1.001**	765.64	763.74	**1.002**	813.58	809.70	**1.005**
R4	664.77	668.92	**0.994**	684.25	687.51	**0.995**	728.89	729.65	**0.999**	773.99	773.70	**1.000**
R5	964.67	944.92	**1.021**	999.21	992.74	**1.007**	1142.17	1127.58	**1.013**	1258.61	1262.50	**0.997**

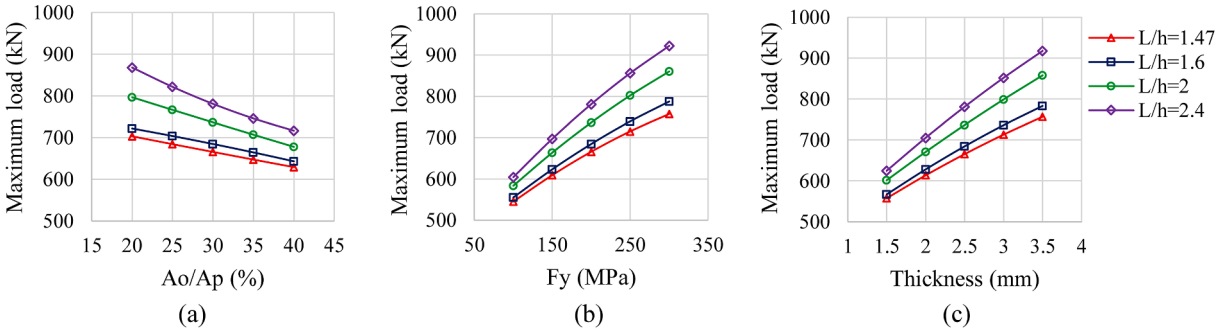

Fig. 9. Variations of the obtained V_{max} from RSM equations for $L/h = 1.47$, 1.6, 2, and 2.4 versus variations of: (a) A_o/A_p, (b) F_y, and (c) Thickness , The hold values are (a) $F_y = 200$ MPa and $t = 2.5$mm, (b) $t = 2.5$mm and $A_o/A_p = 30\%$, and (c) $F_y = 200$ MPa and $A_o/A_p = 30\%$.

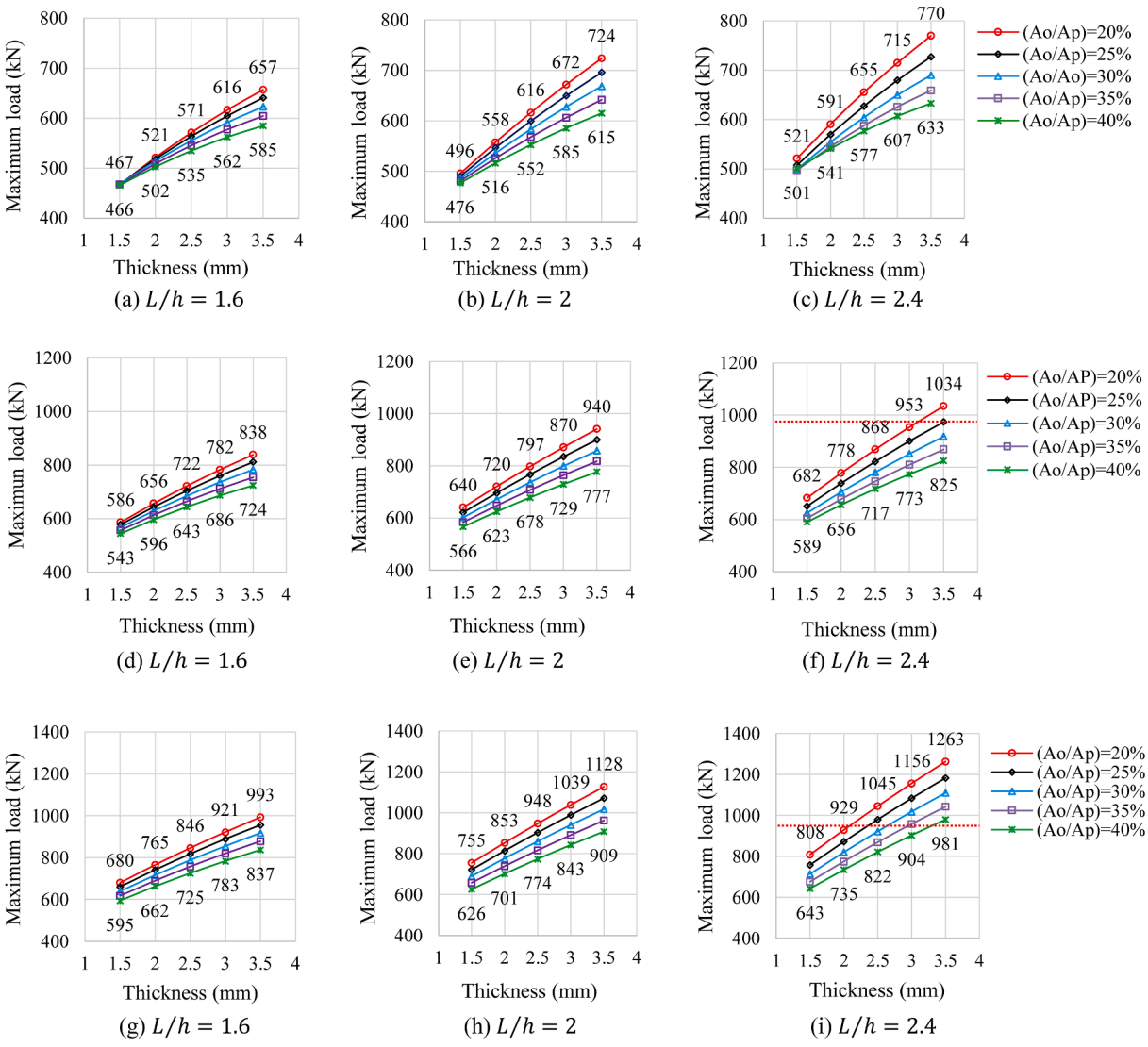

Fig. 10. $V_{max(20\%\leq A_o/A_p\leq 40\%)}$ versus variations of thickness in $L/h = 1.6$, 2, and 2.4: (a), (b), and (c) are for $F_y = 100$ MPa, (d), (e), and (f) are for $F_y = 200$ MPa, (g), (h), and (i) are for $F_y = 300$ MPa.

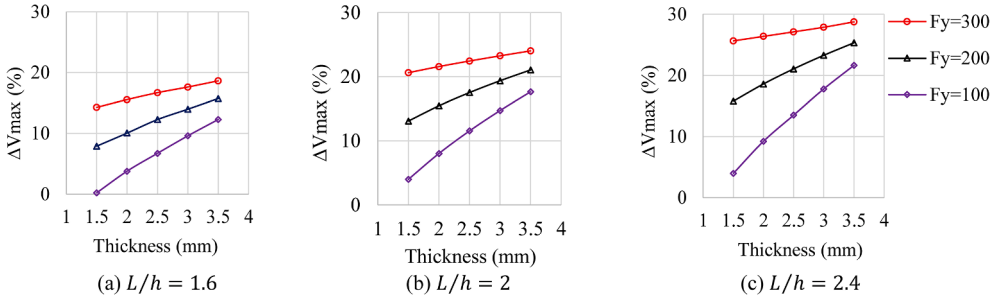

Fig. 11. Comparison of $\Delta V_{\max(20\%<A_o/A_p<40\%)}$ versus variations of thickness in $F_y = 100, 200, and\ 300\ MPa$ for: (a) $L/h = 1.6$, (b) $L/h = 2$, and (c) $L/h = 2.4$.

1.6, 2, and 2.4 are shown in Fig. 11. $\Delta V_{\max(20\%<A_o/A_p<40\%)}$ is calculated by considering the difference of $V_{\max}$ in maximum and minimum value of A_o/A_p $(i.e.(V_{max20\%} - V_{max40\%})/V_{max40\%})$ for different L/h (according to Fig. 10). As shown in this Figure, in all thicknesses of the infill plate, increasing L/h results in rising in $\Delta V_{\max(20\%<A_o/A_p<40\%)}$. This indicates that by increasing L/h of the specimens, the effects of A_o/A_p on V_{max} is increased. In addition, Fig. 11 illustrates that, in different L/h, the sensitivity of specimens to variations of the infill plate thickness decreases by increasing F_y.

6. Conclusions

In this study, the shear behavior of stiffened steel plate shear walls (SSPSWs) with rectangular openings was investigated using response surface method (RSM), in which nonlinear finite element (NLFE) analysis results used as input data. Effect of different parameters on the shear

capacity (V_{max}) of SSPSW was studied. The investigated parameters were, yielding stress (F_y), thickness (t) and opening ratio (A_o/A_p) of the steel infill plate. In addition, aspect ratios of the infill plate were considered as $L/h = 1.47$, 1.6, 2, and 2.4. Using RSM results, regression equations and graphs (see Fig. 10) were proposed, in which by having characteristics of specimens such as the aspect ratio of L/h and F_y, the optimum size of openings and thickness of the infill plate can be selected to find the desired shear capacity. The main results of this study can be summarized as follows:

- Comparing the results of FEM and RSM in terms of the V_{max} indicated negligible difference between values of the two methods. Results demonstrated that, RSM can predict the V_{max} of the specimens, accurately.
- The sensitivity of the V_{max} is moderately higher for F_y than A_o/A_p.
- In the all aspect ratios, variations of the V_{max} have linear relationship with variations of the steel infill plate thickness. In addition, effect of variations of A_o/A_p on variations of the V_{max} is more noticeable in the models with higher thickness of infill plate.
- By increasing L/h of the specimens, the effects of A_o/A_p on the V_{max} is increased. In addition, for different L/h, sensitivity of the specimens to variations of the thickness of the infill plate decreases by increasing F_y.

CRediT authorship contribution statement

Maryam Bypour: Validation, Writing - original draft, Writing - review & editing, Conceptualization, Data curation, Software, Resources. **Mahdi Kioumarsi:** Supervision, Methodology, Data curation, Software, Conceptualization, Writing - review & editing. **Mohammad Yekrangnia:** Software, Writing - review & editing, Resources.

Declaration of Competing Interest

The authors declare that they have no known competing financial interests or personal relationships that could have appeared to influence the work reported in this paper.

Appendix A. Supplementary material

Supplementary data to this article can be found online at https://doi.org/10.1016/j.engstruct.2020.111340.

References

[1] AISC A. AISC 341–10. Seismic provisions for structural steel buildings. Chicago, IL: American Institute of Steel Construction; 2010.
[2] Driver RG, Kulak GL, Kennedy DL, Elwi AE. Cyclic test of four-story steel plate shear wall. J Struct Eng 1998;124:112–20.
[3] Sabouri-Ghomi S, Ventura CE, Kharrazi MH. Shear analysis and design of ductile steel plate walls. J Struct Eng 2005;131:878–89.
[4] Bypour M, Gholhaki M, Kioumarsi M, Kioumarsi B. Nonlinear analysis to investigate effect of connection type on behavior of steel plate shear wall in RC frame. Eng Struct 2019;179:611–24.
[5] Bypour M, Kioumarsi B, Kioumarsi M. Investigation of failure mechanism of thin steel plate shear wall in RC frame. Key Engineering Materials: Trans Tech Publ; 2019. p. 314–21.
[6] Qi Y, Gu Q, Sun G, Zhao B. Shear force demand on headed stud for the design of composite steel plate shear wall. Eng Struct 2017;148:780–92.
[7] Zirakian T, Zhang J. Structural performance of unstiffened low yield point steel plate shear walls. J Constr Steel Res 2015;112:40–53.
[8] Yamaguchi T, Takeuchi T, Nagao T, Suzuki T, Nakata Y, Ikebe T et al. Seismic control devices using low-yield-point steel. Nippon Steel Technical Report Overseas; 1998: 65-72.
[9] Berman JW, Bruneau M. Experimental investigation of light-gauge steel plate shear walls for the seismic retrofit of buildings; 2003.
[10] Roberts TM, Sabouri-Ghomi S. Hysteretic characteristics of unstiffened perforated steel plate shear panels. Thin Wall Struct 1992;14:139–51.
[11] Vian D. Steel plate shear walls for seismic design and retrofit of building structures. State University of New York at Buffalo; 2005.
[12] Bhowmick AK, Grondin GY, Driver RG. Nonlinear seismic analysis of perforated steel plate shear walls. J Constr Steel Res 2014;94:103–13.
[13] Meghdadian M, Gharaei-Moghaddam N, Arabshahi A, Mahdavi N, Ghalehnovi M. Proposition of an equivalent reduced thickness for composite steel plate shear walls containing an opening. J Constr Steel Res 2020;168:105985.
[14] Formisano A, Lombardi L, Mazzolani F. Perforated metal shear panels as bracing devices of seismic-resistant structures. J Constr Steel Res 2016;126:37–49.
[15] Meghdadian M, Ghalehnovi M. Effects of the opening on the behavior of Composite Steel Plate Shear Wall (CSPSW). J Rehabilit Civ Eng 2019;7:139–52.
[16] Meghdadaian M, Ghalehnovi M. Improving seismic performance of composite steel plate shear walls containing openings. J Build Eng 2019;21:336–42.
[17] Bypour M, Kioumarsi M, Zucconi M. Effect of stiffeners on behavior of steel plate shear wall with rectangular openings. In: 17th international conference of numerical analysis and applied mathematics, Greece; 2019.
[18] Alavi E, Nateghi F. Experimental study on diagonally stiffened steel plate shear walls with central perforation. J Constr Steel Res 2013;89:9–20.
[19] Formisano A, Lombardi L, Mazzolani FM. Full and perforated metal plate shear walls as bracing systems for seismic upgrading of existing rc buildings. Ingegneria Sismica 2016;33:16–34.
[20] Nassernia S, Showkati H. Experimental study of opening effects on mid-span steel plate shear walls. J Constr Steel Res 2017;137:8–18.
[21] Sabouri-Ghomi S, Mamazizi S. Experimental investigation on stiffened steel plate shear walls with two rectangular openings. Thin Wall Struct 2015;86:56–66.
[22] Hosseinzadeh S, Tehranizadeh M. Introduction of stiffened large rectangular openings in steel plate shear walls. J Constr Steel Res 2012;77:180–92.
[23] Shafaei S, Farahbod F, Ayazi A. Concrete stiffened steel plate shear walls with an unstiffened opening. Structures: Elsevier; 2017. p. 40-53.
[24] Council A. Guidelines for cyclic seismic testing of component of steel structures. Redwood City, CA: ATC-24; 1992.
[25] Adkins KA. A model for prediction of fracture initiation in finite element analyses of welded steel connections. University of Cincinnati; 2014.
[26] Kioumarsi MM, Hendriks MA, Geiker MR. Quantification of the interference of localised corrosion on adjacent reinforcement bars in a concrete beam in bending. Nordic Concrete Research (NCR). 2014;49:39–57.
[27] Du Y, Clark LA, Chan AH. Impact of reinforcement corrosion on ductile behavior of reinforced concrete beams. ACI Struct J 2007;104:285.
[28] Kallias A, Rafiq MI. Performance assessment of corroding RC beams using response surface methodology. Eng Struct. 2013;49:671–85.
[29] Hooshmandi S, Kioumarsi B, Kioumarsi M, Hajmohammadian Baghban M. Application of response surface method (RSM) on sensitivity analysis of reinforced concrete bridge pier wall; 2017.
[30] Myers RH, Montgomery DC. Anderson cook, CM: Response Surface Methodology: Process and Product Optimization Using Designed Experiments. New York: John Wiley & Sons; 2009.
[31] Agency FEM. NEHRP recommended provisions for seismic regulations for new buildings and other structures. Fema 2003.
[32] ANSI A. AISC 341-05: Seismic provisions for structural steel buildings. American Institute of Steel Construction Inc, American Institute of Steel Construction, Chicago, IL; 2005.